

Comparison of Image Quality According To Application of CT Algorithms for Acquisition of Clinical Information: A Phantom Study

GuiChul Lee^{1,2}, DongKyoon Han³, JooWan Hong^{3*}

1. Department of Radiology, Seoul National University Bundang Hospital, 82, Gumi-ro 173beon-gil, Bundang-gu, Seongnam-si, Gyeonggi-do, 13620, Republic of Korea
2. Department of Radiology, Graduate School, Eulji University, Republic of Korea
3. Department of Radiological sciences, College of Health Sciences, Eulji University, Seongnam-si, Gyeonggi-Do, 13135, Republic of Korea

ARTICLE INFO

Article type:
Original Paper

Article history:

Received: Apr 14, 2022
Accepted: July 17, 2022

Keywords:

Spectral CT
Hounsfield Unit
SNR
Metal Reduction
Monoenergetic Imaging

ABSTRACT

Introduction: While various algorithms are applied in acquiring diagnostic information during computed tomography, such algorithms may affect image quality. The present study aimed to investigate the changes in image quality according to the application of the metal reduction algorithm and monoenergetic image in standard imaging.

Material and Methods: Spectral computed tomography was used to acquire images with the application of standard, metal artifact reduction, monoenergetic, and monoenergetic+metal artifact reduction under the same conditions according to without or with of metal in ACR phantom. ImageJ program was used to measure the HU, noise, and SNR of polyethylene, bone, and acrylic located inside the ACR phantom using the same-sized ROIs.

Results: HU measurement results showed changes in all materials, except acrylic with metal artifacts in the images. Moreover, the results showed a decrease in HU in images with the application of monoenergetic. Noise measurement results also showed changes in all materials, except acrylic with metal artifacts in the images. Moreover, the results showed a decrease in noise in images with the application of monoenergetic. For SNR measured relative to standard images, the results showed degradation of image quality due to a decrease of 36.5–77.7% in SNR and an increase in error value in all materials except acrylic. Whereas, acrylic showed an increase of 3.2–4.1% and a decrease in error values, resulting in improved image quality.

Conclusion: Therefore, it is believed that the accuracy of reading could be increased by considering the changes in image quality and characteristics when applying algorithms for acquiring clinical information from CT.

► Please cite this article as:

Lee G, Han D, Hong J. Comparison of Image Quality According To Application of CT Algorithms for Acquisition of Clinical Information: A Phantom Study. Iran J Med Phys 2023; 20: 153-158. 10.22038/IJMP.2022.64957.2114.

Introduction

In modern medicine, computed tomography (CT) plays a very important role in the diagnosis of diseases through the diversification of basic imaging, contrast media, and examination techniques. Moreover, images used in the diagnosis are being used as the means for providing effective information for disease treatments, such as surgery and radiation therapy. To provide such information in an effective and timely manner, CT technology has been upgraded to enable shorter examination time and acquisition of high-quality images owing to advances in hardware, such as improved X-ray generation efficiency and detector performance and increased gantry rotation speed, as well as advances in software with the application of various algorithms, such as metal artifact removal and spectral based image (SBI). In particular, the development and application of various

algorithms is providing various information during image reading together with standard CT [1, 2]. Metal placed inside the body, such as a dental implant or artificial joint, acts as a factor that degrades CT image quality and interferes with anatomical determination. Meanwhile, metal reduction algorithms with iterative filtering and model-based iterative reconstruction (MBIR) for differentiating metal-only images and tissue images are used on CT sinograms to prevent information loss in CT images due to metal, which is widely used for image reading in radiology and treatment planning for radiation therapy [3-5]. Moreover, monoenergetic images using the individual characteristics of high- and low-energy X-rays through SBI acquired using dual-source CT are used for diagnosis and metal artifact reduction (MAR) [6,7]. Advances in CT technology are being utilized usefully

*Corresponding Author: Tel: +82-10-3213-2326; Fax: +82-31-740-7380; Email: wani9387@gmail.com

during image, reading for disease diagnosis [8,9]. However, images with the application of the algorithm using raw data can be beneficial for diagnosis and treatment planning, but such application may cause changes in image quality [10]. CT has developed and applied various algorithms suitable for inspection purposes due to the development of image processing algorithms as well as hardware performance improvement. Typical examples are soft, standard, detail, bone, lung, edge algorithms, etc., depending on the examination site, metal reduction using repeated reconstruction, monoenergetic spectral CT, and Image processing using software such as reconstruction using artificial intelligence (AI) is being used [11]. Although such a software algorithm is appropriately applied depending on the type of examination, when the algorithm is combined and used, the quality of the image may change and affect the diagnosis. Accordingly, the present study aimed to identify changes in image quality according to the application of MAR and monoenergetic algorithms in CT images.

Materials and Methods

Image acquisition

CT images with the application of different algorithms were acquired under the same conditions using dual-layer detector spectral CT (iQon Spectral CT, Philips Healthcare). Among American College of Radiology (ACR) accreditation phantoms (Gammex ACR 464, Sun Nuclear, Florida, USA), module 1 was used. Phantoms without metal inserted into the air hole and with metal (Lipowitz's alloy, Bi 50%, Pb 26.7%, Sn 13.3%, Cd 10%) inserted into the air hole using a 3D printer (Ultimaker S5, Netherlands) were used (Table 1 and Figure 1). The binder for fixing the metal was prepared using polylactic acid (PLA). Each phantom was used to acquire data from standard images with no algorithm applied and images with application of MAR,

monoenergetic, and monoenergetic and MAR algorithms applied. For monoenergetic, single energy (70 keV) was used.

Image quality assessment

For image quality assessment, measurements were made using polyethylene, bone, and acrylic located inside the ACR phantom module 1. ImageJ program (National Institutes of Health, ver. 1.8.0_172) was used for the measurements with ROIs set for each material. Because the air measurement part in the ACR phantom module 1 is the binding site for artificially generating metal artifacts, it was excluded from the image quality assessment.

For the assessment of HU accuracy, phantoms w/ metal and w/o metal with the application of standard MAR, monoenergetic, and monoenergetic+MAR were repeatedly scanned 10 times. HU of polyethylene, bone, and acrylic inside ACR phantom module 1 was measured and calculated using the following equation [12].

$$\text{Hounsfield Unit} = 1000 \cdot \frac{\mu_{\text{tissue}} - \mu_{\text{water}}}{\mu_{\text{water}}} \quad (1)$$

Here, μ_{tissue} is the tissue attenuation coefficient, and μ_{water} is the water attenuation coefficient.

For the assessment of noise in the acquired CT images, phantoms w/ metal and w/o metal with the application of standard, MAR, monoenergetic, and monoenergetic+MAR were repeatedly scanned 10 times. SD of polyethylene, bone, and acrylic inside ACR phantom module 1 was measured and calculated using the following equation [13].

$$\text{Noise}(\sigma) = \sqrt{\frac{\sum(X_i - \bar{X})^2}{n-1}} \quad (2)$$

Here, X_i is the independent pixel value, \bar{X} is the mean pixel value, and n is the total number of pixels.

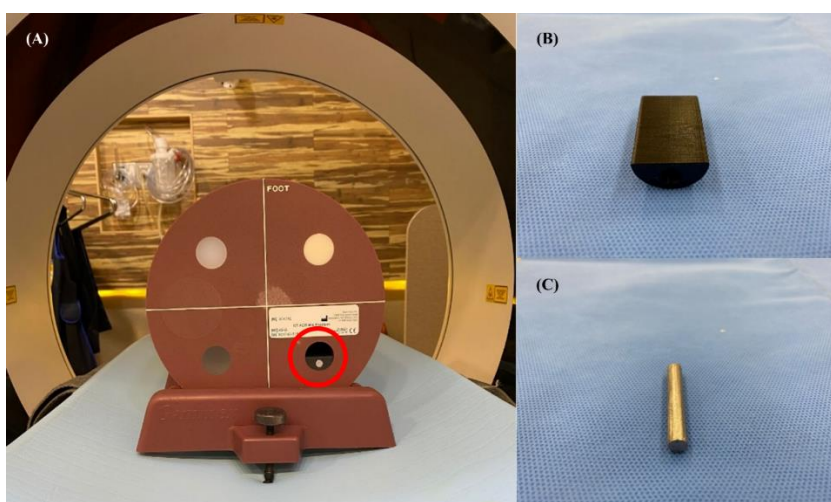


Figure 1. Installation of phantom for experiments. (A) Was ACR phantom in house-made 3D printer holder, (B) was house-made 3D printer holder, (C) was Lipowitz's alloy

For the assessment of SNR, standard, phantoms w/ metal and w/o metal with application of standard, MAR, monoenergetic, and monoenergetic+MAR were repeatedly scanned 10 times. SNR, peak SNR (PSNR), root mean square error (RMSE), and mean absolute error (MAE) of an image of the entire ACR phantom and polyethylene, bone, and acrylic inside module 1 were compared relative to standard images. SNR and PSNR were calculated using the following equations [13].

$$SNR[dB] = 10 \cdot \log\left(\frac{P_{signal}[\omega]}{P_{noise}[\omega]}\right) \quad (3)$$

Here, $P_{signal}[\omega]$ is the signal intensity and $P_{noise}[\omega]$ is the noise intensity [14].

$$PSNR = 10 \log \frac{S^2}{MAE} \quad (4)$$

Here, S^2 is the peak signal and MAE is the mean absolute error.

Table 1. CT scan parameters of image acquisition

Parameters	Value / Mode
Dose right	Off
kV / mAs	120 / 150
Rotation time(sec)	0.5
Collimation(mm)	64 X 0.625
Pitch / Scan increment	0.985
Scan mode	Helical scan
Reconstruction mode	iDose4
Filter	Y-sharp(YA)
Thickness(mm)	2
Increment(mm)	2

Statistical analysis

Statistical data analysis on experimental results was performed using SPSS (IBM SPSS Statistics, SPSS for Windows ver. 22, Chicago, IL). Differences according

to an algorithm in phantoms w/ metal and w/o metal were analyzed using Kruskal-Wallis one-way analysis of variance and pairwise comparison post-hoc test. Results with p -value < 0.05 were considered to be statistically significant.

Results

Images of phantoms w/ metal and w/o metal for image quality assessment and each ROI image for image quality assessment were as follows (Figure 2).

With respect to HU values of phantoms w/ metal and w/o metal with the application of an algorithm, the results showed a statistically significant difference in HU values ($p < 0.05$), except acrylic ($p = 0.06$). Moreover, pairwise comparison post-hoc test results showed no statistically significant differences in HU values of all materials, except acrylic, in phantoms w/ metal among standard images without the application of monoenergetic algorithm and images with the application of MAR, monoenergetic, and monoenergetic+MAR algorithm applied. The results confirmed changes in HU values according to the application of monoenergetic algorithm ($p > 0.05$). However, acrylic of phantoms w/metal showed no changes in HU values according to the algorithm ($p = 0.06$), whereas images with the application of monoenergetic algorithm showed changes in HU values ($p = 0.007$) (Table 2).

With respect to SD values of phantoms w/ metal and w/o metal with the application of an algorithm, the results showed statistically significant differences ($p < 0.05$), except acrylic ($p = 0.22$). Moreover, the pairwise comparison post-hoc test showed no statistically significant differences in SD values in standard images without the application of monoenergetic algorithm and images with the application of MAR, monoenergetic, and monoenergetic+MAR algorithm applied. The results confirmed changes in SD values according to the application of monoenergetic algorithm ($p > 0.05$) (Table 3).

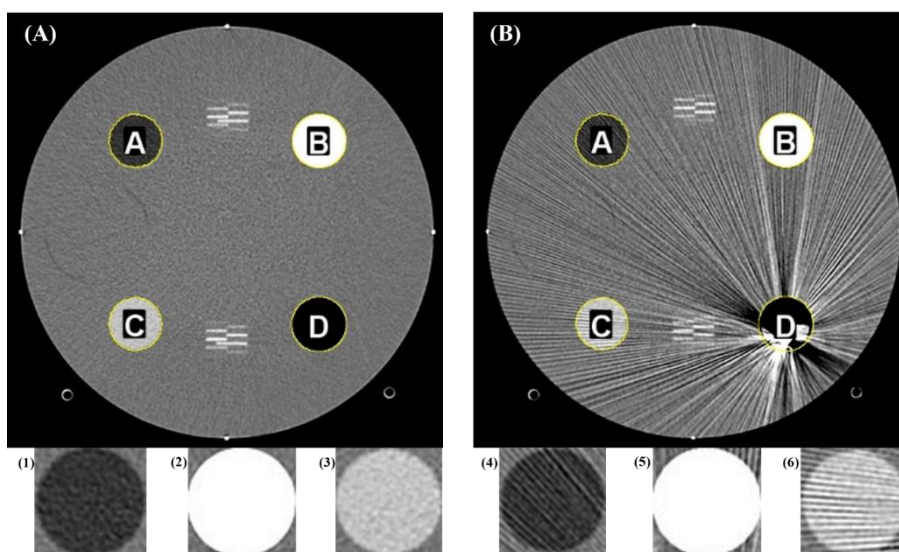


Figure 2. ACR phantom CT scan images. (A) was without metal(w/o metal) and (1)~(3) was the ROIs for measurement was polyethylene, bone, acrylic in order. (B) was with metal(w/ metal) and (4)~(6) was the ROIs for measurement was polyethylene, bone, acrylic in order.

Table 2. Results of hounsfield unit for applied algorithms (Unit: HU)

Image	ROIs	Algorithms				p-value		
		Standard	MAR	monoenergetic	monoenergetic+MAR			
w/o metal phantom	Poly-ethylene	-89.1±1.54	-89.1±1.54	-65.4±0.70	-65.4±0.70	0.00*	0.985§	0.939¶
	Bone	879.5±7.63	879.5±7.63	470.0±2.99	470.0±2.99	0.00*	0.985§	0.969¶
	Acrylic	119.2±2.50	119.2±2.50	126.3±1.18	126.3±1.18	0.00*	0.985§	0.939¶
w/ metal phantom	Poly-ethylene	-88.1±0.93	-86.7±0.89	-65.6±1.14	-63.5±0.78	0.00*	0.146§	0.157¶
	Bone	870.8±6.38	877.1±6.25	466.2±2.83	468.5±2.84	0.00*	0.267§	0.4¶
	Acrylic	121.9±2.87	119.4±3.44	123.9±1.59	120.9±1.18	0.06*	0.121§	0.007¶

p-value* was kruskal-wallis one-way analysis of variance, p-value§ was pairwise comparison post-hoc test for Non and MAR images, p-value¶ was pairwise comparison post-hoc test for monoenergetic and monoenergetic + MAR

Table 3. Results of SD for applied algorithms

Image	ROIs	Algorithms				p-value		
		Standard	MAR	monoenergetic	monoenergetic+MAR			
w/o metal phantom	Poly-ethylene	19.6±0.40	19.6±0.40	12.9±0.30	12.8±0.30	0.00 *	0.985§	1.00¶
	Bone	230.3±1.82	230.3±1.82	129.2±0.98	129.2±0.98	0.00 *	1.00§	0.985¶
	Acrylic	23.0±0.59	23.0±0.59	24.8±0.63	24.8±0.63	0.00 *	0.969§	0.969¶
w/ metal phantom	Poly-ethylene	36.4±6.83	33.7±6.14	25.9±4.92	24.0±4.75	0.00 *	0.349§	0.433¶
	Bone	228.7±1.57	231.1±1.59	130.9±2.79	131.6±2.53	0.00 *	0.157§	0.566¶
	Acrylic	70.3±12.98	66.8±11.90	65.1±11.32	62.5±10.95	0.22 *	0.22§	0.22¶

p-value* was kruskal-wallis one-way analysis of variance, p-value§ was pairwise comparison post-hoc test for Non and MAR images, p-value¶ was pairwise comparison post-hoc test for monoenergetic and monoenergetic+MAR

Table 4. Results of SNR, PSNR, RMSE, MAE for applied algorithms

Evaluation index	Image	ROIs	Algorithms			
			MAR	monoenergetic	monoenergetic+MAR	
SNR	w/o	Whole	29.9±0.31	20.2±0.29	20.2±0.28	
		Polyethylene	130.4±0.26	9.5±0.66	9.5±0.72	
		metal	Bone	29.9±1.18	6.7±0.13	6.7±0.11
			Acrylic	14.9±0.26	15.4±1.82	15.5±1.97
	w/	Whole	20.9±1.40	17.4±1.03	17.3±0.45	
		Polyethylene	11.2±4.80	7.5±1.22	7.1±1.27	
		metal	Bone	27.9±3.55	6.6±0.99	6.7±0.10
			Acrylic	12.3±4.46	7.9±1.64	7.8±1.38
PSNR	w/o	Whole	44.8±0.32	35.1±0.29	35.1±0.28	
		Polyethylene	8.6±1.09	5.0±1.28	5.0±1.30	
		metal	Bone	32.3±1.19	9.0±0.11	9.0±0.09
			Acrylic	19.0±0.24	19.6±1.86	19.6±2.01
	w/	Whole	35.8±1.40	32.3±1.02	32.2±0.45	
		Polyethylene	13.3±4.48	9.7±2.53	9.3±2.53	
		metal	Bone	30.7±3.53	9.4±0.23	9.5±0.25
			Acrylic	19.9±4.14	15.6±2.06	15.4±1.58
RMSE	w/o	Whole	17.8±0.63	54.3±1.83	54.2±1.74	
		Polyethylene	17.9±0.51	26.9±2.01	27.0±2.04	
		metal	Bone	25.9±3.92	374.8±8.83	374.8±7.65
			Acrylic	19.1±0.48	18.3±3.41	18.2±3.60
	w/	Whole	50.2±8.25	75.4±9.27	75.9±3.89	
		Polyethylene	26.6±10.23	36.6±4.62	38.4±6.02	
		metal	Bone	34.2±12.09	372.1±6.66	369.6±7.02
			Acrylic	34.1±12.97	51.0±8.29	52.2±8.63
MAE	w/o	Whole	13.7±0.46	21.8±1.91	21.8±1.91	
		Polyethylene	14.3±0.42	23.4±1.01	23.4±1.05	
		metal	Bone	20.9±3.47	326.9±8.08	326.9±6.89
			Acrylic	15.2±0.36	14.8±2.39	14.7±2.62
	w/	Whole	28.8±7.86	40.0±5.30	40.6±3.40	
		Polyethylene	21.3±8.23	29.9±3.29	31.4±4.39	
		metal	Bone	27.2±9.87	326.5±5.81	324.7±6.07
			Acrylic	27.4±10.28	40.9±6.88	42.1±7.32

With respect to SNR and PSNR values of phantoms w/ metal and w/o metal with the application of an algorithm, the results showed degradation of image quality with a decrease in values in all materials, except acrylic of phantom w/o metal. The maximum difference in SNR values was -77.7% in polyethylene for phantom w/o metal and -36.5% in acrylic for phantom w/ metal phantom. The maximum difference in PSNR values occurred in bone for both with -72.1% and -69.2%. However, the values increased in acrylic, 4.1% in phantom w/o metal and 3.2% in phantom w/ metal, to show improvement in image quality. RMSE and MAE also increased in all materials, except acrylic of phantom w/o metal, and as a result, degradation in image quality occurred due to an increase in error values (Table 4).

Discussion

The present study investigated the changes in image quality according to the application of various algorithms depending on the situation when acquiring CT images. The experimental results showed significant changes in HU, SD, SNR, PSNR, RMSE, and MAE values according to the algorithm in all materials, except acrylic. Of these, images with the application of monoenergetic algorithm showed degradation of image quality as compared to standard images. Algorithms applied during CT examinations clearly offer many benefits. MAR, which uses an iterative reconstruction technique, can effectively remove metal artifacts while also reducing scattering and beam hardening, and thus, it can be used to simulate regions that may be obscured by artifacts [15-17]. In the present study, images with the application of MAR showed effective removal of metal artifacts without significant changes to the image quality, such as HU, noise, and SNR, as compared to standard images. Meanwhile, monoenergetic algorithm can be used to optimize intravascular iodine using mono-energy in the low-energy region, while mono-energy in the high-energy region is effective for metal artifact reduction [18, 19]. However, the findings in the present study showed that it had an influence on the degradation of image quality, such as HU, noise, and SNR, as compared to standard images. According to a study by Wichmann, using a mono-energy of 60 keV during the interpretation of head and neck cancer can significantly improve the overall image quality [20]. However, due to the characteristics of monoenergetic algorithm that uses mono-energy, degradation of image quality occurred due to the total amount of photons used for image generation is small. Moreover, a study by Albrecht reported that a decrease in CNR and SNR occurred at the 40-60 keV energy range, as compared to mono-energy of 70 keV, which confirmed that using higher mono-energy caused greater degradation of the quality of diagnostic images [21, 22]. Similarly, the MAR algorithm using high-energy monoenergetic showed effective metal artifact reduction, but compared to standard images, changes in HU in inside materials were larger, and a decrease in SNR caused an increase in noise. As mentioned earlier, monoenergetic algorithm

can increase the contrast enhancement effect and reduce metal artifacts, but because mono-energy is used, degradation of image quality relative to standard images occurs. Therefore, when using this algorithm in clinical practice, where accurate disease diagnosis is required, sufficient understanding and awareness of this algorithm are needed. During diagnosis using CT images with the application of various algorithms, such images should be used as reference data, together with standard images, for accurate diagnosis. The limitations of the present study included the fact that phantom images, rather than actual patient images, were used. Moreover, the experiment was not conducted with a varying energy range of monoenergetic. Furthermore, the study also did not check changes in the shape of surrounding structures according to the application of the algorithm. Therefore, additional studies with varying mono-energy ranges are needed in the future.

Conclusion

The findings in the present study confirmed that it is possible to use various information needed for diagnosis and increase the accuracy of image reading by considering the changes in image quality and characteristics of algorithms used during CT image acquisition. However, changes in image quality that may occur when such algorithms are applied should be considered when reading images to acquire clinical information.

Acknowledgment

This paper was supported by the eulji university in 2018 (EJRG-18-06) and this work was supported by the Ministry of Education of the Republic of Korea and the National Research Foundation of Korea (NRF-2019R1G1A1010922)

References

1. Lell MM, Kachelrieß M. Recent and upcoming technological developments in computed tomography: high speed, low dose, deep learning, multienergy. *Investigative radiology*. 2020 Jan 1;55(1):8-19.
2. Nielsen JS, Van Leemput K, Edmund JM. MR-based CT metal artifact reduction for head-and-neck photon, electron, and proton radiotherapy. *Medical physics*. 2019 Oct;46(10):4314-23.
3. Hong J, Choi J, Kim K, Ahn J. Evaluation of Radiation Treatment Planning By Computed Tomography Metal Artifact Reduction Algorithm. *Iranian Journal of Medical Physics*. 2021 Nov 1;18(6).
4. Zhang Y, Yan H, Jia X, Yang J, Jiang SB, Mou X. A hybrid metal artifact reduction algorithm for x-ray CT. *Medical physics*. 2013 Apr;40(4):041910.
5. Healthcare P. Metal artifact reduction for orthopedic implants (O-MAR). White Paper, Philips CT Clinical Science, Andover, Massachusetts. 2012.
6. Albrecht MH, Vogl TJ, Martin SS, Nance JW, Duguay TM, Wichmann JL, et al. Review of clinical applications for virtual monoenergetic dual-energy CT. *Radiology*. 2019 Nov;293(2):260-71.

7. Pessis E, Sverzut JM, Campagna R, Guerini H, Feydy A, Drape JL. Reduction of metal artifact with dual-energy CT: virtual monospectral imaging with fast kilovoltage switching and metal artifact reduction software. In: *Seminars in musculoskeletal radiology*. 2015 ; 19(05): 446-55.
8. Kwon H, Kim KS, Chun YM, Wu HG, Carlson JN, Park JM, et al. Evaluation of a commercial orthopaedic metal artefact reduction tool in radiation therapy of patients with head and neck cancer. *The British journal of radiology*. 2015 Aug;88(1052):20140536.
9. Kwan AC, Pourmorteza A, Stutman D, Bluemke DA, Lima JA. Next-generation hardware advances in CT: cardiac applications. *Radiology*. 2021 Jan;298(1):3-17.
10. Batawil N, Sabiq S. Hounsfield unit for the diagnosis of bone mineral density disease: a proof of concept study. *Radiography*. 2016 May 1;22(2):e93-8.
11. Gjestebj L, Yang Q, Xi Y, Zhou Y, Zhang J, Wang G. Deep learning methods to guide CT image reconstruction and reduce metal artifacts. *Physics of medical imaging*. 2017 Mar 10132:752-8
12. Ye N, Jian F, Xue J, Wang S, Liao L, Huang W, et al. Accuracy of in-vitro tooth volumetric measurements from cone-beam computed tomography. *American journal of orthodontics and dentofacial orthopedics*. 2012 Dec 1;142(6):879-87.
13. Verdun FR, Racine D, Ott JG, Tapiovaara MJ, Toroi P, Bochud FO, et al. Image quality in CT: From physical measurements to model observers. *Physica Medica*. 2015 Dec 1;31(8):823-43.
14. Diwakar M, Kumar M. A review on CT image noise and its denoising. *Biomedical Signal Processing and Control*. 2018 Apr 1;42:73-88.
15. Diwakar M, Kumar M. A review on CT image noise and its denoising. *Biomedical Signal Processing and Control*. 2018 Apr 1;42:73-88.
16. Cherala G, Sharma S, Chhabra A. Dual energy CT in musculoskeletal applications beyond crystal imaging: bone marrow maps and metal artifact reduction. *Skeletal radiology*. 2022 Aug;51(8):1521-34.
17. Katsura M, Sato J, Akahane M, Kunimatsu A, Abe O. Current and novel techniques for metal artifact reduction at CT: practical guide for radiologists. *Radiographics*. 2018 Mar;38(2):450-61.
18. Al-Baldawi Y, Hokamp NG, Haneder S, Steinhäuser S, Püsken M, Persigehl T, et al. Virtual monoenergetic images and iterative image reconstruction: abdominal vessel imaging in the era of spectral detector CT. *Clinical Radiology*. 2020 Aug 1;75(8):641-e9.
19. Gao Z, Meng D, Lu H, Yao B, Huang N, Ye Z. Utility of dual-energy spectral CT and low-iodine contrast medium in DIEP angiography. *International Journal of Clinical Practice*. 2016 Sep;70(9B):B64-71.
20. Wichmann JL, Nöske EM, Kraft J, Burck I, Wagenblast J, Eckardt A, et al. Virtual monoenergetic dual-energy computed tomography: optimization of kiloelectron volt settings in head and neck cancer. *Investigative radiology*. 2014 Nov 1;49(11):735-41.
21. Albrecht MH, Scholtz JE, Hüßers K, Beeres M, Bucher AM, Kaup M, et al. Advanced image-based virtual monoenergetic dual-energy CT angiography of the abdomen: optimization of kiloelectron volt settings to improve image contrast. *European radiology*. 2016 Jun;26:1863-70.
22. Neuhaus V, Hokamp NG, Abdullayev N, Rau R, Mpotsaris A, Maintz D, et al. Metal artifact reduction by dual-layer computed tomography using virtual monoenergetic images. *European journal of radiology*. 2017 Aug 1;93:143-8.